Soft Matter

PERSPECTIVE

Cite this: *Soft Matter*, 2019, **15**, 1902

Designing biomimetic liquid diodes

Jiaqian Li,[a] Yuxin Song,[a] Huanxi Zheng,[a] Shile Feng,[a] Wanghai Xu[a] and Zuankai Wang *[ab]

Received 11th January 2019,
Accepted 5th February 2019

DOI: 10.1039/c9sm00072k

rsc.li/soft-matter-journal

Just as the innovation of electronic diodes that allow the current to flow in one direction provides a foundation for the development of digital technologies, the engineering of surfaces or devices that allow the directional and spontaneous transport of fluids, termed liquid diodes, is highly desired in a wide spectrum of applications ranging from medical microfluidics, advanced printing, heat management and water collection to oil–water separation. Recent advances in manufacturing, visualization techniques, and biomimetics have led to exciting progress in the design of various liquid diodes. In spite of exciting progress, formulating a general framework broad enough to guide the design, optimization and fabrication of engineered liquid diodes remains a challenging task to date. In this review, we first present an overview of the development of biological and engineered liquid diodes to elucidate how to control the surface chemistry and topography to regulate the transport of liquids without the need for external energy. Then the latest design strategies allowing for the creation of longitudinal and transverse liquid diodes are discussed and compared. We also define some figures of merit such as the rectification coefficient and the transport velocity and distance to quantify the performance of liquid diodes. Finally, we highlight perspectives on the development of engineered liquid diodes that transcend nature and adapt to various practical applications.

1. Introduction

The directional and passive transport of water droplets is a ubiquitous phenomenon in nature and plays a crucial role in various practical applications in the areas of energy, physics, chemistry, materials, medicine and biology.[1–14] Analogous to electronic diodes that conduct an electric current preferentially in one forward direction while blocking in the reverse direction (Fig. 1a), a fluidic device that rectifies a liquid to directionally flow could be considered as a 'liquid diode' (Fig. 1b). Distinct from electronic diodes that work based on semiconductor materials by application of an external voltage, an ideal liquid diode is capable of directionally transporting fluid based on various materials without the need for any external energy input (Table 1). In addition, in striking contrast to electronic diodes which have been mature building blocks of digital technology, the design, fabrication, quantification and optimization of fluid diodes remain elusive (Fig. 1a).

The first engineered passive liquid diode dates back to 1992 with the introduction of a gradient surface by heterogeneously modifying the chemical properties of a smooth silicon wafer[15] (Fig. 2). The creation of a chemical gradient builds a pressure difference around the droplet, resulting in a typical trait of unidirectional liquid transport toward the more wettable area. But this type of engineered liquid diode is usually restricted by relatively large hysteresis resistance stemming from the direct contact between a liquid and a solid, as well as the easy decay of the chemical monolayer in long-term operation. Over the course of evolution, nature has developed diverse, almost-perfect structures allowing for the preferential mass and energy transport of various droplets involving multiple sources, scales and dynamics, as exemplified by static nanoscale dews and fast millimeter-scale raindrops. Through the comprehensive bottom-up exploration of living creatures, such as desert beetles, shorebirds, spiders, cacti, lizards and pitcher plants[16–24] (yellow timeline in Fig. 2), the preferred transport of droplets on these biological surfaces is found to be mainly attributed to the evolved topographical structures with delicate scales, curvatures, shapes, roughness and arrangements, as well as asymmetric wettability properties. Under the inspiration of these biological surfaces and the myriad requirements of practical applications, the field of engineered liquid diodes has flourished over the past three decades[25–47] (green and gray timelines in Fig. 2). These biomimetic liquid diodes learn from nature, and imitate the exquisite morphology and composition of biological surfaces to attain superior traits of directional liquid transport in either longitudinal or transverse directions.

Over the past several years, extensive progress in the understanding of biological liquid diodes and the creation of engineered

[a] *Department of Mechanical Engineering, City University of Hong Kong, Hong Kong 999077, China*
[b] *Shenzhen Research Institute of City University of Hong Kong, Shenzhen 518057, China. E-mail: zuanwang@cityu.edu.hk*

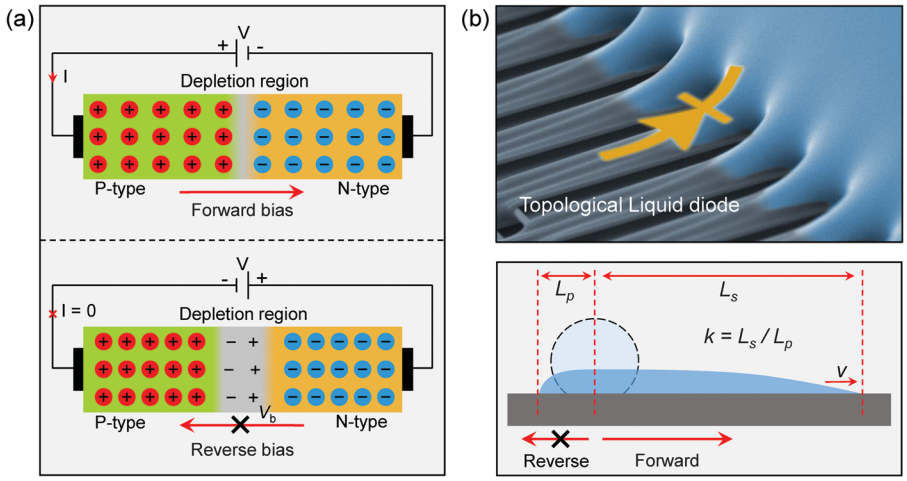

Fig. 1 Comparison between electronic diodes and liquid diodes. (a) Schematic diagrams for electronic diodes to elucidate the diode principles in the forward and reverse directions. Here V, I and V_b are the voltage, current and breakdown voltage in the electronic diode. (b) Schematic diagrams for liquid diodes allowing preferential droplet transport in a single direction. The top is one of the most representative liquid diodes and the bottom schematic presents some important parameters in the system of liquid diodes. Here k, v, L_p and L_s represent the rectification coefficient, transport velocity in the forward direction, transport distance in the backward direction, and spreading distance in the forward direction, respectively.

Table 1 Comparison between electronic diodes and liquid diodes

	Electronic diodes	Liquid diodes
Carrier	Electrons and holes	Liquids
Material	Semiconductors	Most materials
Energy	Apply a forward bias	No external energy input
Control mechanism	Doping	Chemistry and topography

counterparts has been made; however, formulating a general route broad enough to guide rational design remains a challenging task. In spite of limitless inspiration from nature, the direct transfer of delicate topographies and profound principles learned from diverse biological surfaces into artificial devices might not give rise to the best solutions. Thus, advances in knowledge learned through predictive understanding or empirical study, manufacturing and visualization are equally important. In addition, both natural and practical systems involve a diversity of environmental conditions; unidirectional liquid transport might only function under a specific condition. Thus, it is important to build a comprehensive framework to guide the design, manufacture, quantification and optimization of engineered liquid diodes for various practical applications.

In this review, we first present the fundamentals for the design of liquid diodes and the important milestones related to biological and engineered liquid diodes. We then focus on the latest biomimetic strategies to design longitudinal and transverse liquid diodes, and compare their directional transport performance. We conclude this review by suggesting challenges in and perspectives on the future development of engineered liquid diodes before practical applications.

2. Fundamentals

The design and optimization of liquid diodes require basic understanding of interfacial wetting dynamics, a phenomenon

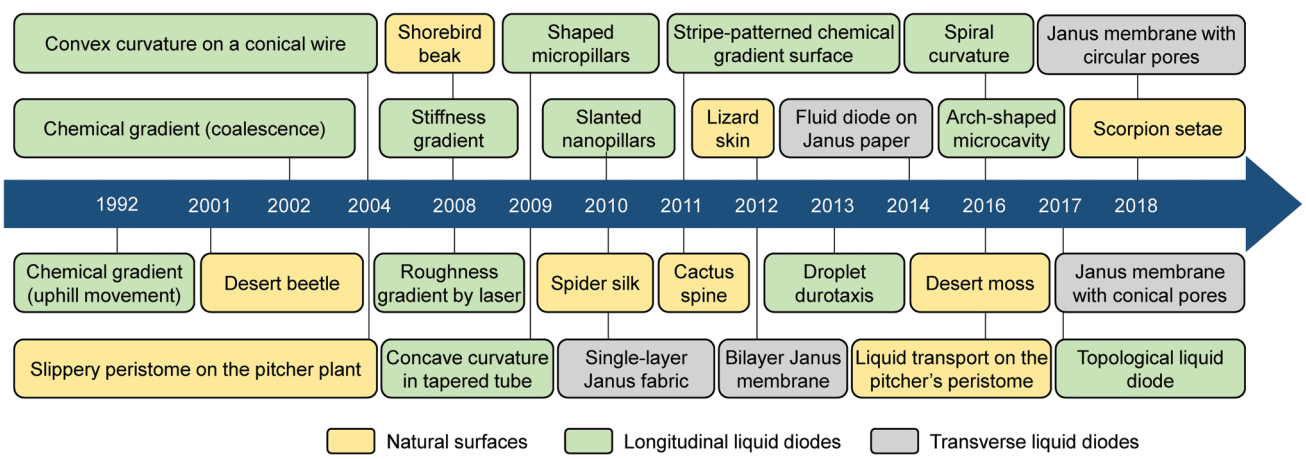

Fig. 2 Timeline of major advances in the area of liquid diodes. Yellow zones represent the development of natural liquid diodes. Green and gray zones represent the major advances of engineered liquid diodes, including longitudinal liquid diodes (green zones) and transverse liquid diodes (gray zones).

occurring between a liquid and a solid surface. Wetting also plays a vital role in a variety of large-scale applications, such as anti-fouling on submarines, anti-icing on airplanes, and self-cleaning on textiles, as well as in micro and nanoscience, such as nanoemulsion separation, microfluidics and nanoprinting.

The basic framework of wetting was laid down by Thomas Young[48] in 1805, who proposed the contact angle (CA) to quantify the equilibrium state of a droplet on a smooth surface.[48] Based on the specific value of the CA (θ), a surface can be categorized into hydrophilic ($\theta < 65^\circ$) or hydrophobic ($\theta > 65^\circ$). Although a simple measurement of the CA using standard equipment directly reveals the wetting property of a surface, the contact angle, by its essence, is simply a reflection of the static, macroscopic behavior of a material. Instead, the contact angle hysteresis (CAH),[49] defined as the difference between the advancing contact angle and the receding contact angle, is more related to the microscopic features of a surface and also more accurately reveals the global mobility of a liquid droplet on a surface.[50–52] Later, the emergence of Wenzel[53] and Cassie–Baxter[54,55] equations significantly extended our understanding of how surface roughness regulates the variation of surface wettability. All together, these advances provide important insights into how to design surfaces with desired properties, ranging from superhydrophilicity ($\theta \leq 5^\circ$) to superhydrophobicity ($\theta \geq 150^\circ$ and CAH $\leq 5^\circ$).

A key breakthrough in the understanding of wetting is the elucidation of the self-cleaning mechanism responsible for lotus leaves that grow in mud.[56,57] Although the beauty of a liquid pearl on a lotus leaf was documented one thousand years ago by a Chinese poet, it was not until 1997 that the secret underlying this peculiar property was first revealed. Triggered by this breakthrough, a great raft of superhydrophobic surfaces have been created on various materials such as metals, graphene, polymers and glasses, manifesting a wide spectrum of topological structures such as pillars, bumps, cavities, fibers, spines and grooves.[58–60] In one extreme case, from the static wetting perspective, liquid repellency even to low-surface-energy liquids can be achieved by the delicate control of surface morphology, such as re-entrant and double re-entrant structures.[61–66] At the other extreme, from the dynamic wetting perspective, robust water repellency with the shortest contact time can be achieved by elegantly designing surfaces which can efficient rectify capillary energy into kinetic energy.[67,68] As a result, the droplet can exhibit spectacular pancake bouncing, a phenomenon that fundamentally breaks the physical contact limit of a bouncing droplet.[69–72]

As an alternative to superhydrophobic surfaces, another type of special wetting which can deliver superior liquid mobility is slippery liquid-infused porous surfaces (SLIPs) or liquid-impregnated surfaces (LIS) modeled after pitcher plants.[73–81] This kind of slippery surface takes advantage of a smooth and reconfigurable liquid/liquid interface to replace the conventional triple-phase interface and offers many distinct advantages such as enhanced stability at high pressure and high humidity.

3. Representative liquid diodes in nature

Probably, one of the best strategies for the design of engineered liquid diodes is to learn from nature. Nature has evolved a myriad of biological liquid diodes that give preferential fluid transport in various ways.[82,83] In spite of the diversity and complexity, the design principles that underpin these biological liquid diodes are universal.

Desert beetles are one of the most studied biological examples that harness a wettability gradient to guide the transport of a liquid. In the Namib desert, some beetles[16] (Fig. 3a) collect drinking water from the morning fog by virtue of their bumpy backs, which consist of wax-free hydrophilic peaks and wax-coated hydrophobic troughs and slopes. Such a wettability gradient between peaks and troughs gives rise to a special droplet-collection system, in which droplets either grow and accumulate on the hydrophilic peaks or move from hydrophobic regions to the hydrophilic peaks.

A structural curvature gradient also serves as an effective route on natural liquid diodes. Careful observations revealed that some shorebirds[20] (Fig. 3b) can move droplets mouthward because of the geometry of their open beak, which creates a surface-tension-induced transport of droplets under the cooperation of a concave curvature gradient and mechanical tweezing motion. Following this study, natural water collection systems on spider silk (Fig. 3c, 2010),[18] cactus spines (Fig. 3d, 2011),[19] desert moss (Fig. 3e, 2016),[23] and scorpion setae[24] (Fig. 3f, 2018) were successively reported as shown in Fig. 2. They are capable of capturing water efficiently either from fog in humid air or dew through nucleation by virtue of the structural topography. Although these natural surfaces feature complex and hierarchical topography, they have a common conical shape with a convex curvature gradient, which is different from the concave curvature gradient inside a shorebird beak. Both concave and convex curvature gradients can produce a gradient of Laplace pressure around the deposited droplet. Under the effect of a Laplace pressure gradient, a droplet on a conical structure can move from the tip (larger curvature) to the base (smaller curvature) whereas a droplet deposited inside a conical cavity or corner moves from the wider side (smaller curvature) to the narrower side (larger curvature). More notably, spider silk (Fig. 3c) perfectly combines a wettability gradient and structural curvature in its water collection system. Spider silk is composed of spindle-knots interwoven with highly random nanofibrils and joints made of relatively aligned nanofibrils (Fig. 3c), which means that the spindle-knot is more hydrophilic than the joint. As a result, the seamless integration between the wettability gradient and structural curvature drives the droplets to accumulate around the spindle-knots, building a continuous effective water collection system.

Biological surfaces also take advantage of asymmetric structures to rectify the transport of the droplet. The most representative examples using this strategy are the skin of desert lizards (Fig. 3g) and the peristome of pitcher plants (Fig. 3h). Lizards[21,84] that live in arid areas have evolved polygon-shaped scales on their body to collect water from rain or moisture. A network of interconnected asymmetric capillary channels formed between the scales is responsible for directionally transporting the collected water

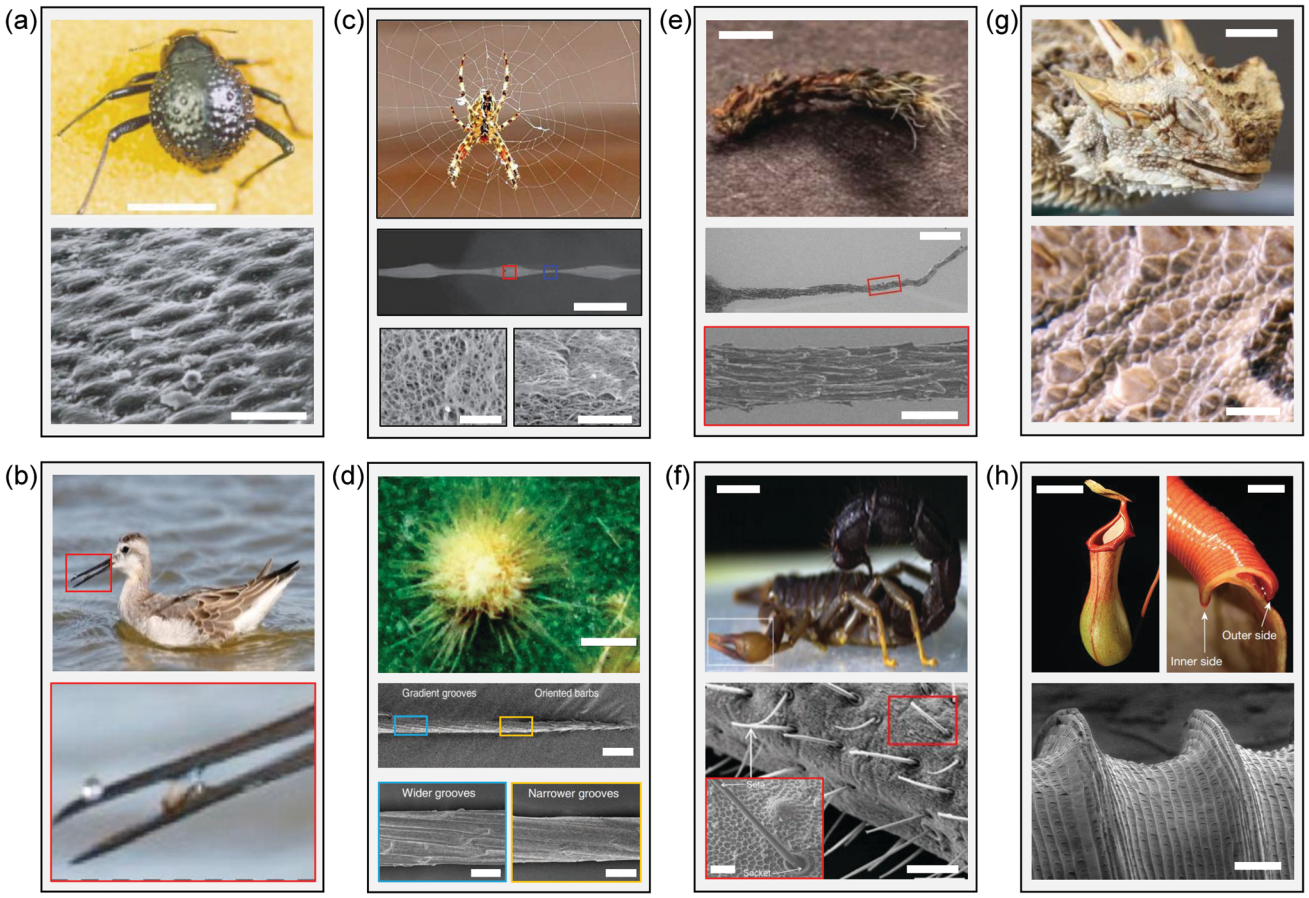

Fig. 3 Representative liquid diodes in nature. (a) Namib desert beetle. The bumpy back of the beetle consists of wax-free hydrophilic peaks and wax-coated hydrophobic troughs and slopes. (b) Shore bird Wilson's phalarope. The droplets move mouthward because of the geometry of the open beak and mechanical tweezing motion. (c) Spider silk. Spider silk is composed of spindle-knots made of random nanofibrils (bottom left) and joints made of aligned nanofibrils (bottom right). (d) Cacti. Cactus spines contain three integrated parts with different topographical features, oriented barbs at the tip, gradient grooves in the middle, and belt-structured trichomes at the base. (e) Desert moss. The awn of desert moss continually tapers towards the distal end and possesses unique multiscale micro- and nanogrooves. (f) Desert scorpions. The setae of desert scorpions have a small conical shape, which is covered by parallel channels and ridges with an exquisite linear alternating distribution. (g) Desert lizards. A network of interconnected asymmetric capillary channels forms between the scales of lizards. (h) Pitcher plants. The pitcher's rim consists of a wide range of relatively large microgrooves covered by elegant small microgrooves and asymmetric arch-shaped microcavities. Scale bars: (a) top 10 mm, bottom 10 μm; (c) middle 50 μm, bottom 1 μm; (d) top 500 μm, middle 100 μm, bottom 20 μm; (e) top 2 mm, middle 200 μm, bottom 50 μm; (f) top 10 mm, bottom 100 μm, inset 50 μm; (g) top 5 mm, bottom 2 mm; (h) top left 5 cm, top right 1 cm, bottom 200 μm. Figures reproduced with permission from: (a) ref. 16, Copyright (2001) Macmillan Publishers Limited; (b) ref. 20, Copyright (2008) AAAS; (c) ref. 5 and 18, Copyright (2010) Macmillan Publishers Limited and Copyright (2018) The Royal Society of Chemistry; (d) ref. 19, Copyright (2012) Macmillan Publishers Limited; (e) ref. 23, Copyright (2016) Macmillan Publishers Limited; (f) ref. 24, Copyright (2018) Wiley-VCH; (g) ref. 84, Copyright (2011) Beilstein-Institut; (h) ref. 22 and 86, Copyright (2016) Macmillan Publishers Limited and Copyright (2018) Springer Nature Limited.

toward the snout for survival. Similarly, pitcher plants that grow in tropical areas have also developed a distinctive peristome surface to transport liquid directionally from the inner side to the outer side of the peristome.[22,85] This pitcher's rim consists of a wide range of relatively large microgrooves covered by elegant small microgrooves and asymmetric arch-shaped microcavities (Fig. 3h). Both the width and the depth of the large microgrooves gradually diverge from the inner side to the outer side, creating a unique roughness gradient.[86] The seamless cooperation between the capillary rise inside the microcavities and the capillary gradient inside large microgrooves is responsible for preferential droplet spreading in the direction toward the outer side, while sharp edges are present for strong pinning in the reverse direction. Recent experiments further show that the manifestation of unidirectional droplet spreading on the peristome surface is intricately dependent on the interplay between the multiscale physical structures and multiscale sources of water, such as rain, fog and dew.[86] Moreover, the directional transport of a liquid on the peristome surface collapses under some conditions, for example, when a falling droplet with a high Weber number impacts on the peristome surface.[86]

4. Biomimetic liquid diodes

Boosted by the understanding of the basic mechanisms underlying biological examples and spurred on by potential practical applications including water harvesting, microfluidics and

advanced printing, extensive efforts have been devoted to the development of engineered liquid diodes. In spite of extensive advances, to completely replicate superior functions from nature using an effective and facile method remains challenging. In applications, engineered liquid diodes are preferred to transport virtually any kind of liquids on various materials, such as fabrics, polymers, plastics, glass and metal, as well as in various configurations, such as fibers, channels, membranes and tubes. Thus, the development of ideal engineered liquid diodes not only requires the perfect transfer of nature's principles, but also needs adaptation to various materials and configurations in a robust way. From the perspective of the rectification direction of a liquid, we divide biomimetic liquid diodes into two categories (Fig. 4). The first type is longitudinal liquid diodes, on which a droplet is preferentially transported in a single direction along the surface (Fig. 4a and b), and the other is transverse liquid diodes (Fig. 4c) which are characterized by directional liquid flow across the surface.

To better guide the design, we first elaborate several parameters related to the quantification of liquid diodes. The first one is the rectification coefficient, which is defined as the spreading distance in the forward direction (L_s) relative to that in the reverse direction (L_p), expressed as $k = L_s/L_p$ (Fig. 1b). A larger rectification coefficient represents a high ability to rectify a liquid. The transport distance and velocity (L_s and v in Fig. 1b) are also important characteristics to quantify the transport properties. Generally, it is difficult to achieve a long transport distance and high velocity on a single liquid diode simultaneously owing to the tradeoff between the driving force and hysteresis resistance.

4.1. Longitudinal liquid diodes

On the basis of the contact line features during the dynamic transport of a droplet, we classify longitudinal liquid diodes into two modes, slip-mode liquid diodes (Fig. 4a) and spreading-mode liquid diodes (Fig. 4b). In the slip mode, the advancing and receding contact lines of the droplet move almost simultaneously in one direction (Fig. 4a), whereas the contact line of the droplet just propagates in one direction and pins in all others in the spreading mode (Fig. 4b).

4.1.1. Slip-mode liquid diodes. Slip-mode liquid diodes mainly take advantage of a wettability gradient or curvature gradient to transport a liquid in a preferential direction. The former generally stems from the variation of surface energy on a two-dimensional (2D) surface, while the curvature gradient results from the asymmetric structure of a one-dimensional (1D) material. Both of them give rise to a pressure gradient around the droplet, breaking the symmetry of the contact line to produce their directional transport of liquid.

A. Wettability gradient. One of the most facile strategies to design slip-mode liquid diodes is a wettability gradient, including a chemical gradient (Fig. 5a), a roughness gradient (Fig. 5b) and a stiffness gradient (Fig. 5c). A chemical gradient involves a gradual variation in the chemical characteristics of one or more chemical species on the substrate (Fig. 5a right).[15,87–93] Chaudhury *et al.*[15] first developed a slip-mode liquid diode using the strategy of a chemical gradient that was fabricated by heterogeneous vapor diffusion of a decyltrichlorosilane monolayer on a flat silicon surface.

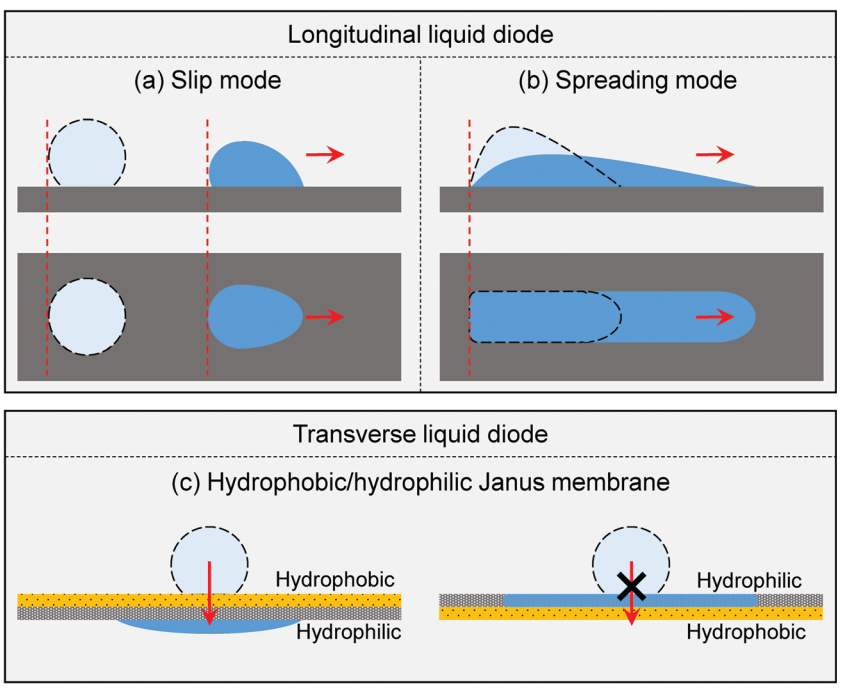

Fig. 4 Schematic diagrams for longitudinal and transverse liquid diodes. (a and b) Schematics for longitudinal liquid diodes, consisting of slip mode (a) and spreading mode (b). In the slip mode, the advancing and receding contact lines of a droplet move almost simultaneously in one direction, while in the spreading mode, the contact line of a droplet just spreads in one direction but pins in all others. (c) Schematics for transverse liquid diodes on hydrophobic/hydrophilic Janus membranes. A droplet directionally penetrates from the hydrophobic side to the hydrophilic side, while being blocked in the reverse direction.

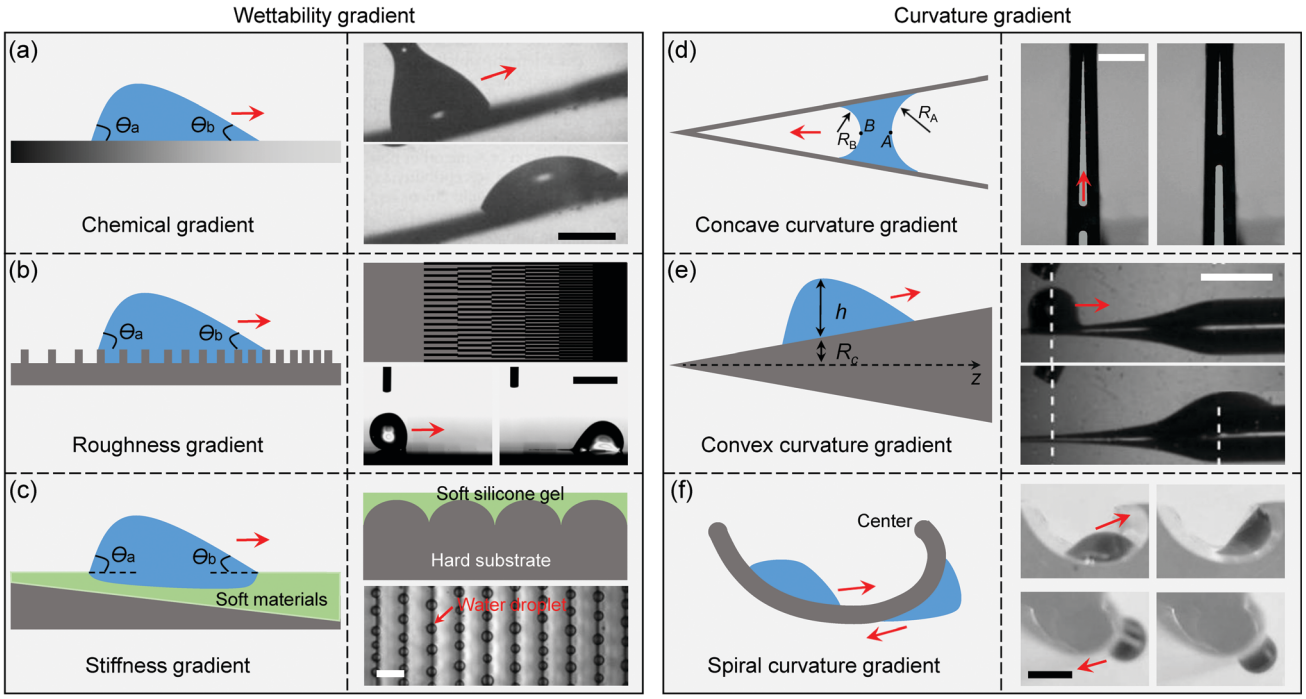

Fig. 5 Principle schematics and corresponding representative slip-mode liquid diodes. (a) Schematic diagram (left) and optical images (right) showing directional droplet transport on a liquid diode with a chemical gradient. (b) Schematic diagram (left) revealing directional droplet transport on a liquid diode with a roughness gradient and optical images (right) showing a large roughness gradient from superhydrophobic to hydrophilic by etching silicon nanopillars and adjusting the area of a black hydrophilic stripe. (c) Schematic images showing the mechanism of a stiffness gradient (left) and an optical image that displays the large-scale droplet pattern through the regulation of the stiffness of the substrate (right). (d) Schematic diagram (left) and optical images (right) showing directional droplet transport on a liquid diode with a concave curvature gradient. (e) Schematic diagram (left) revealing the mechanism of a convex curvature gradient and optical images (right) showing ultrafast droplet transport on a liquid diode through the careful regulation of a smooth tapered tube. (f) Schematic (left) and optical (right) images showing directional droplet transport on spiral structures. Scale bars: (a) 1 mm; (b) 2 mm; (c) 170 μm; (d) 2 mm; (e) 2 mm; (f) 2 mm. Figures reproduced with permission from: (a) ref. 15, Copyright (1992) AAAS; (b) ref. 34, Copyright (2017) Springer Nature Limited; (c) ref. 41, Copyright (2013) National Academy of Sciences; (d) ref. 120, Copyright (2014) American Chemical Society; (e) ref. 38, Copyright (2014) American Physical Society; (f) ref. 40, Copyright (2016) Springer Nature Limited.

This slip-mode liquid diode was able to transport a droplet uphill with an average velocity of 1–2 mm s^{-1} (Fig. 5a left), and also rectify the random movements of condensate droplets into a collective motion with a faster speed hundreds to thousands of times than those of typical Marangoni flows.[94] In addition to harnessing a single chemical monolayer, a chemical gradient can also be fabricated by patterning two different monolayers, such as hydrophobic fluorinated stripes and hydrophilic silica stripes.[87,88] The majority of chemical gradients[89–93] are developed based on the techniques of self-assembled monolayers (SAMs) of silane molecules.[95,96] But, the SAMs-based technique gives rise to incomplete and discontinuous chemical monolayers, which decay in long-term operation and induce a larger hysteresis to impede the motion of a liquid.

Unlike a chemical gradient, a roughness gradient produces a relatively stable wettability gradient for the creation of slip-mode liquid diodes[33,34,97–104] (Fig. 5b). The movement of a droplet on a surface with a roughness gradient is usually accompanied by a wetting transition from a Cassie–Baxter state to a Wenzel state. Such a transition leads to a large increase of the hysteresis resistance, which stops the self-motion of the droplet unless external energy is applied.[33,105–107] Thus, a large roughness gradient should be built to surmount the hysteresis resistance[34] (Fig. 5b right). Moreover, the delicate control of topographical roughness can also create slip-mode liquid diodes for the directional transport of oils and other liquids with lower surface tension, which remains a challenge to date.[108]

A stiffness gradient offers another available route to design slip-mode liquid diodes[41,109–111] (Fig. 5c). Distinct from a hard substrate, a droplet would deform the underlying soft substrate and thus modify the contact line under the interplay between capillary force and elastic force.[112–114] As a result, a stiffness gradient on a soft substrate shows a remarkable ability to regulate the slip of the droplet toward the region with smaller rigidity which features a larger deformation (Fig. 5c left).[111] Through the careful modulation of the substrate stiffness, a large-scale droplet pattern on the soft substrate can be obtained, defined as "droplet durotaxis"[41] (Fig. 5c right).

B. Structural curvature. Compared with a wettability gradient on a two-dimensional surface, curvature gradients mostly exist on 1D asymmetric structures, such as conical fibers, tapered tubes and spiral cantilevers,[24,35–38,40,115–122] which are mainly fabricated using glass, polymers, metal and wood. This kind of curvature gradient has been widely harnessed to design

slip-mode liquid diodes for diverse applications, such as water collection and oil–water separation.[123–127]

One of the curvature gradients for the creation of slip-mode liquid diodes is a concave curvature gradient, which widely exists inside tapered tubes and corners. When placed in an open, tapered capillary tube, a droplet moves spontaneously toward the tip of the tube because of the difference in Laplace pressure between two concave menisci[36,120–122] on its leading and trailing edges (Fig. 5d left). If the bond number is small, the pressure gradient between the two concave menisci can be expressed as $\Delta P = P_A - P_B = 2\gamma(1/R_B - 1/R_A)$, which guides the droplet to slip from the large side to the small side of the tube. Here P_A and P_B are the pressure at point A and B, and R_A and R_B are the meniscus radii at point A and point B, respectively (Fig. 5d left). Similarly, a liquid droplet deposited between two nonparallel plates also displays a directional slip motion toward the region of maximum confinement[37,120] (Fig. 5d right).

In addition to a convex curvature gradient, slip-mode liquid diodes also take advantage of a convex curvature gradient to guide the motion of a liquid (Fig. 5e). In 2004, Quéré *et al.*[35] fabricated a slip-mode liquid diode using a convex curvature gradient on a tapered copper wire. In contrast to a cylindrical wire, the conical wire creates a pressure gradient along the droplet, written as $\left.\frac{dP}{dz}\right|_{\Omega} = -\frac{2\gamma}{(R_c+h)^2}\left(\frac{dR_c}{dz}+\frac{dh}{dz}\right)_{\Omega}$ (Fig. 5e left). Here γ is the surface tension, R_c is the radius of the fiber, h is the maximum thickness of the droplet, and Ω is the volume of the droplet. Under the effect of such a pressure gradient, the droplet slips spontaneously from the tip (large curvature) to the base (small curvature) of the conical wire. More remarkably, carefully controlling the curvature of the structure can give an ultrafast spontaneous motion of micro- and nanoscale droplets on a smooth tapered glass tube.[38] Water droplets on such a slip-mode liquid diode showed a maximum speed of 0.42 m s^{-1}, two orders of magnitude larger than that on the slip-mode liquid diodes using the strategy of a wettability gradient (Fig. 5e right).

Additionally, a special Archimedean spiral structure[40] (Fig. 5f) possesses combined concave and convex curvature, creating a unusual slip-mode liquid diode. On the concave side, a small droplet spontaneously moves toward the center under the effect of the concave curvature gradient. Differently, the droplet deposited on the convex side deviates preferentially from the center owing to the convex curvature gradient (Fig. 5f).

4.1.2. Spreading-mode liquid diodes. Spreading-mode liquid diodes are generally reliant on the design of asymmetric structures on various materials, such as silicon, polymers and photocurable resins.[25,28–30,128–131] In 2010, Wang *et al.*[25] reported the fabrication of slanted silicon micropillars (Fig. 6a), on which the droplet spreads in the direction along the deflection of the nanopillars, but gets pinned in all others. The directional liquid transport on multiscale slanted pillars (Fig. 6a) is dependent on the wetting property of the surface. Multiscale slanted, hydrophilic pillars transport liquid directionally in a small contact angle range, which is determined by the deflection of the pillars and imbibition criterion of the surface. Notably, there is no directional liquid transport on slanted pillars with a superhydrophilic property.

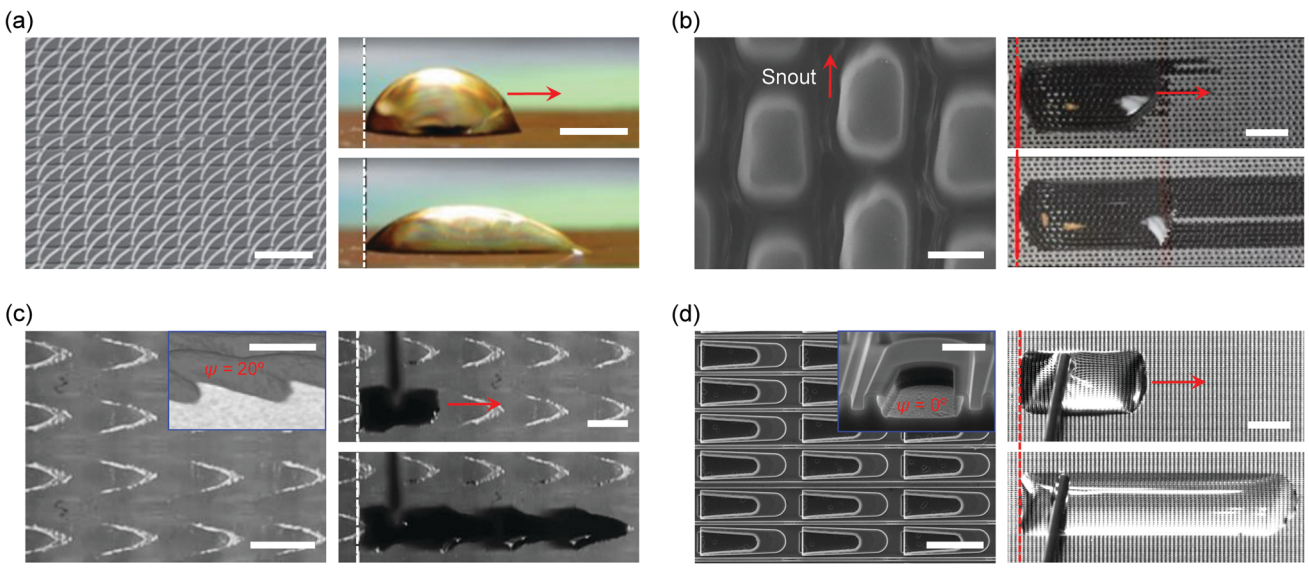

Fig. 6 Engineered longitudinal spreading-mode liquid diodes. (a) Scanning Electron Microscope (SEM) image of slanted nanopillars (left) and the directional spreading behavior of a single droplet (right). (b) SEM image that displays lizard-inspired asymmetric channels (left) and optical images revealing the directional droplet spreading behavior (right). (c) SEM images showing slanted arch-shaped microcavities in microchannels (left) and optical images showing the directional liquid transport on this liquid diode (right). The inset SEM image displays the overhang structures, and ψ is the angle of the overhang ($\psi = 20^\circ$). (d) SEM images showing a topological liquid diode consisting of U-shaped islands in parallel fences (left) and optical images showing the directional liquid transport on this liquid diode (right). The angle of the overhang on this liquid diode is $\psi = 0^\circ$. Scale bars: (a) left 10 μm, right 1 mm; (b) left 200 μm, right 4 mm; (c) left 500 μm, inset 500 μm and right 500 μm; (f) left 100 μm, inset 20 μm and right 1 mm. Figures reproduced with permission from: (a) ref. 25, Copyright (2010) Macmillan Publishers Limited; (b) ref. 141, Copyright (2018) Elsevier; (c) ref. 31, Copyright (2016) Wiley-VCH; (d) ref. 26, Copyright (2017) AAAS.

Additionally, with the input of external energy, such as vibrational and magnetic,[132,133] hydrophobic asymmetric pillars can also rectify the motion of the droplet.

Inspired by desert lizards and pitcher plants, asymmetric channels or cavities[21,25,27–32,84,128–131,133–140] are widely used to create spreading-mode liquid diodes. Inspired by desert lizards, spreading-mode liquid diodes consisting of asymmetric channel networks have been widely developed[21,84,140,141] (Fig. 6b). The channels have a gradient in the width and depth toward the snout along each post, which promotes directional liquid transport in the preferential direction pointing to the snout. But these lizard-inspired liquid diodes also transport the liquid slightly toward the reverse direction,[21,141] showing relatively lower directionality than other liquid diodes. Inspired by pitcher plants, the introduction of an overhang structure can efficiently prevent the transport in the reverse direction of spreading-mode liquid diodes[26,31,32,136,139,142] (Fig. 6c and d), because the overhang structure provides a substantial energy barrier for the pinning of the liquid.[62–65,143,144] Notably, our group[26] has designed and fabricated a novel topological liquid diode (Fig. 6d) by using the standard MEMS technology, which results in superior unidirectional liquid transport with both a relatively high velocity and long distance compared with other engineered liquid diodes reported previously.[21,27–32,84,129–131,135,136,139,140] This topological liquid diode consists of convergent U-shaped island arrays spatially confined in periodically patterned fences. The inner side of the cavity in the U-shaped island is specially decorated by a reentrant structure with an angle of $\Psi = 0^\circ$ (inset in Fig. 6d). The topological surface is also capable of transporting diverse liquids including low-surface-tension liquids such as hexane and high-viscosity liquids such as ethylene glycol, and can even adapt to different working conditions involving microgravity and various transportation routes. More importantly, the topological liquid diode can overcome the undesired Marangoni effect to transport the liquid directionally from the colder zone to the hotter zone, which provides a promising way to solve the dry-out limitation in capillary heat pipes.

4.2. Transverse liquid diodes

Distinct from longitudinal liquid diodes, transverse liquid diodes have a unique trait of directional liquid transportation across membrane materials, such as cell membranes, metal meshes, porous paper and synthetic fabrics.[4,7,145] Two key criteria should be met to construct transverse liquid diodes. One is that the membrane should be thin and porous for easy penetration of the liquid and the other is that the membrane should possess Janus wettability, *e.g.* be hydrophobic on one face and hydrophilic on the other. Under the effect of Janus wettability, a liquid can be transported directionally from the hydrophobic side toward the hydrophilic side of the Janus membrane, while being blocked in the reverse direction (Fig. 3c).

One simple route to obtain transverse liquid diodes is the construction of single-layer hydrophobic/hydrophilic (HP/HL) Janus membranes.[42–44,46,47,146–149] Single-layer Janus membranes can be fabricated by the decoration of one or two sides of homogeneous porous materials, such as fabrics, meshes, paper and sponges. Taking HP/HL Janus fabrics as an example, the water droplet gradually penetrates into the membrane from the hydrophobic side toward the hydrophilic side (Fig. 7a), while it spreads on the hydrophilic side without any permeation in the reverse direction. More remarkably, through mediating the thickness of both hydrophobic and hydrophilic layers, Janus membranes can even overcome gravity to transport a liquid directionally[46,149] (Fig. 7b). Such a directional penetration of the liquid is mainly ascribed to the difference of the breakthrough pressure in two opposite directions, which is dependent on the thickness of the hydrophobic and hydrophilic layers, as well as the pore size and intrinsic wettability. Recent research has revealed that the breakthrough pressure rises significantly with an increase in the thickness of the hydrophobic layer, but is not sensitive to the thickness variation of the hydrophilic layer. Thereby, the design and optimization of transverse liquid diodes requires delicate control of the thickness of the hydrophobic layers of single-layer Janus membranes.

Another route to develop transverse liquid diodes is the design of bilayer HP/HL Janus membranes. A bilayer Janus membrane combines two layers with heterogeneous wettability together and each layer can be fabricated separately.[45,150–152] For example, a transverse liquid diode[45] (Fig. 7c) was fabricated by coupling a fibrous hydrophobic polyurethane (PU) film and a hydrophilic crosslinked poly (vinyl alcohol) (c-PVA) film. This bilayer Janus membrane can rectify a droplet to penetrate from the hydrophobic layer to the hydrophilic layer, but inhibit passing in the reverse direction (Fig. 7c). Compared with single-layer Janus membranes, the breakthrough pressure on bilayer Janus membranes depends not only the thickness of the hydrophobic layer and hydrophilic layer, but also the gap between the two layers. The expanding of the gap increases the breakthrough pressure from the hydrophobic layer to the hydrophilic layer, thereby impeding the directional penetration of the liquid on the transverse liquid diode. Through the coupling of Janus wettability and asymmetric topography, a novel hybrid Janus membrane[152] that efficiently narrows the interval between two layers was recently developed. This hybrid Janus membrane is composed of a hydrophilic copper mesh decorated by nanoneedle arrays and a hydrophobic nanofiber layer. The nanoneedle arrays insert into the micropores on the hydrophobic nanofiber layer, forming an interleaved morphology that remarkably narrows the gap between the hydrophobic layer and the hydrophilic layer. Moreover, these asymmetric nanoneedle arrays induce a Laplace pressure difference, accelerating the directional liquid transport from the hydrophobic layer to the hydrophilic layer. As a result, such a wettability/topography binary cooperative Janus membrane produces relatively superior transport behavior.

4.3. Quantification of liquid diodes

The practical applications of liquid diodes demand sustained and reliable function. However, in certain conditions, such as under a high-speed falling droplet, a negative thermal gradient, or long-term operation, the directional liquid transport capability might decay or become lost. Thus, it is important to quantitatively characterize the dynamic property of a liquid diode.

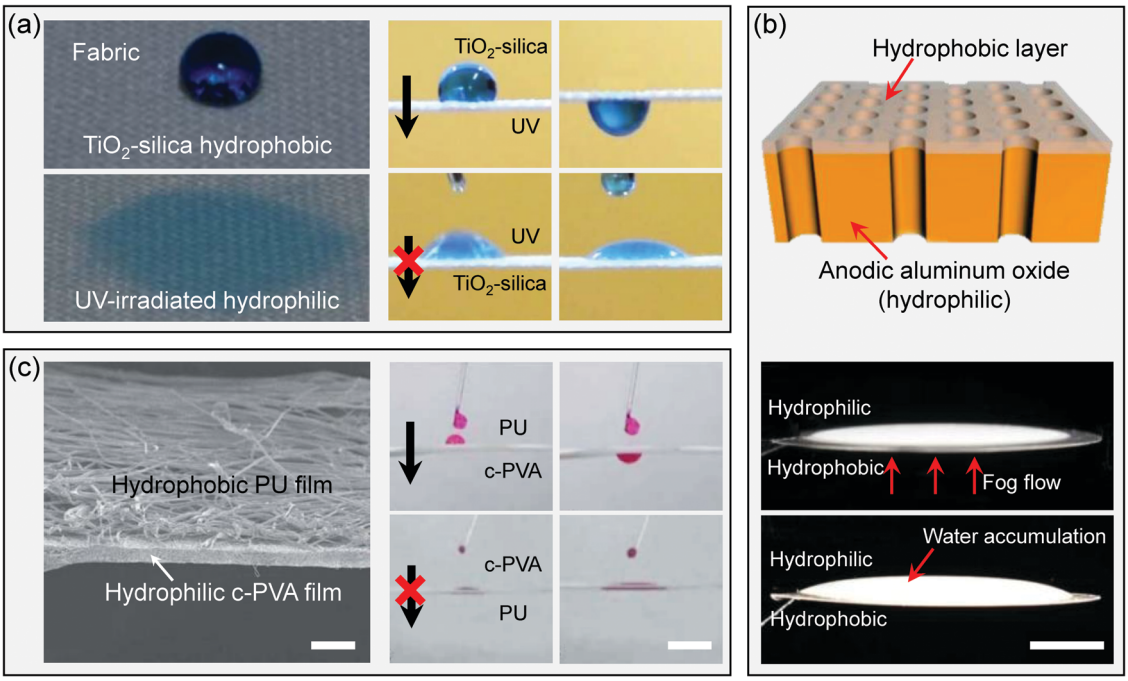

Fig. 7 Representative transverse liquid diodes. (a) Optical images of a single-layer Janus fabric (left) and its directional liquid transport (right). (b) Schematic diagram of a single-layer Janus anodic aluminum oxide membrane with aligned circular micropores (top) and optical images showing the fog collection from the hydrophobic side to the hydrophilic side (bottom). (c) Bilayer Janus membrane consisting of hydrophobic PU film and hydrophilic c-PVA film (left) and the behavior of the directional transport of a water droplet (right). Scale bars: (b) 5 mm; (c) left 10 μm, right 10 mm. Figures reproduced with permission from: (a) ref. 42, Copyright (2010) The Royal Society of Chemistry; (b) ref. 46, Copyright (2018) American Chemical Society; (c) ref. 45, Copyright (2012) The Royal Society of Chemistry.

As defined earlier, the rectification coefficient quantifies the ability of a liquid diode to generate directional liquid transport. In the case of spreading-mode liquid diodes, the released droplet on the lizard-inspired liquid diodes might slightly propagate in the reverse direction, resulting in a lower k. By contrast, spreading-mode liquid diodes inspired by pitcher plants create directional liquid transport with a larger value of k owing to the strong pinning of overhang structures. As such, the rectification coefficient acts as a crucial parameter to measure the capability of spreading-mode liquid diodes. But, the rectification coefficient becomes invalid in the cases of slip-mode liquid diodes and transverse liquid diodes, since these liquid diodes convey the liquid forward over the surface or across the membrane without any reverse backflow, which makes k tend to infinity.

We also compare the average spreading velocity (v) and normalized distance (L_s/R) among various liquid diodes as shown in Fig. 8. Clearly, the use of a wettability gradient can yield a relatively high transport velocity, but a short transport distance (red zone in Fig. 8). Slip-mode liquid diodes with curvature gradients obtain either a high velocity or a long spreading distance (green zones in Fig. 8). It is difficult to achieve both a large velocity and a long distance by taking advantage of a curvature gradient alone. In contrast, the majority of spreading-mode liquid diodes possess a short transport distance and a small velocity simultaneously (blue zone in Fig. 8). The tradeoff between transport velocity and distance can be resolved by the

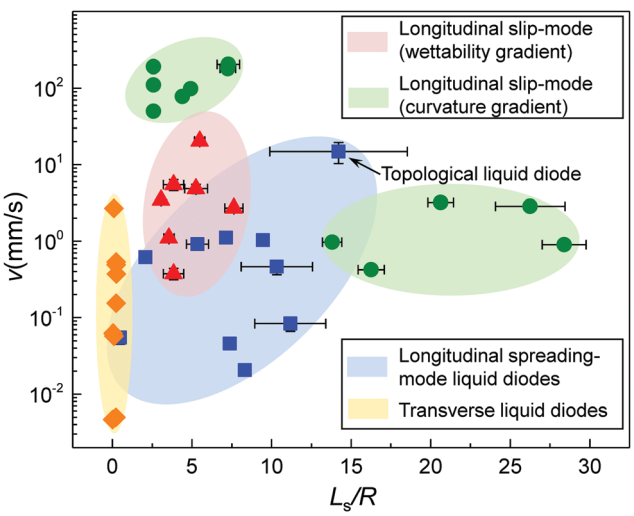

Fig. 8 Comparison of the transport performance among various engineered liquid diodes. A wettability gradient creates directional liquid transport with a relatively high velocity, but a short transport displacement (red zone). A curvature gradient obtains either a high velocity or a long spreading distance (green zones). By contrast, the majority of spreading-mode liquid diodes have a short transport distance and a small transport velocity (blue zone). The tradeoff between the transport velocity and distance can be resolved through the delicate control of asymmetric structures as exemplified by topological liquid diodes. The yellow zone indicates transverse liquid diodes. Here v is the average transport velocity, L_s is the transport distance of a droplet in the forward direction and R is the radius of the droplet.

careful design of asymmetric structures as exemplified by a topological liquid diode that gives both a relatively large velocity and a long distance[26] (Fig. 8). In the case of transverse liquid diodes, the transport distance fails to measure the performance owing to its dependence on the thickness of the Janus membrane. The transport velocity is harnessed to measure the transport efficiency of a droplet from the hydrophobic side to the hydrophilic side[46,47] (yellow zone in Fig. 8). In addition to the transport distance and velocity, some other parameters are generally utilized to evaluate transverse liquid diodes in specific applications, for example, the separation efficiency in oil–water separation and the collection rate in fog collection.

5. Applications of liquid diodes

Liquid diodes have many potential applications owing to their inherent characteristics of rectifying random droplet motion into a collective motion in a specific direction. This advantage is beneficial for a wide range of applications such as water harvesting and thermal management.[123,153–156] In the case of water harvesting, the use of conical structure arrays with a curvature gradient facilitates the directional transport of captured droplets, which creates more free space for subsequent droplet nucleation and capture and results in efficient water harvesting (Fig. 9a).[123] The directional transport of droplets can also promote heat transfer such as in heat pipes. In conventional heat pipes, wicking structures are designed to transport liquid from the condenser to the evaporator, which are severely restricted by the negative temperature gradient as well as the dry-out problem. In contrast, the design of novel topological liquid diodes is capable of combating the negative thermal gradient and allows for the spontaneous rectification of condensate droplets back to the evaporator (Fig. 9b). Such a design provides a promising route to solve the dry-out problem in conventional heat pipes.[155]

Liquid diodes also find potential applications in oil–water separation and functional textiles. For example, HP/HL Janus membranes become selectively permeable to oil or water in an immiscible medium[43,146] with the proper tailoring of the thickness of the hydrophobic and hydrophilic layers. When the hydrophobic side of a Janus membrane is in contact with an oil–water mixture, a water droplet can break through the oil-infused hydrophobic layer to penetrate toward the hydrophilic layer. In the reverse direction, the water droplet tends to spread on the hydrophilic layer without any penetration. Likewise, when the hydrophilic side of a Janus membrane is toward the oil–water mixture, the oil droplet selectively permeates through the Janus membrane without any backflow. Thus, a Janus membrane can selectively remove oil or water from an oil–water mixture and avoid remixing at the same time (Fig. 9c), in contrast to conventional homogeneous hydrophobic or hydrophilic membranes. In the same way, a functional bandage fabricated from a HP/HL Janus membrane efficiently drains excess biofluid away from wounds and prevents backflow simultaneously, which is of benefit in accelerating the process of wound healing[157] (Fig. 9d).

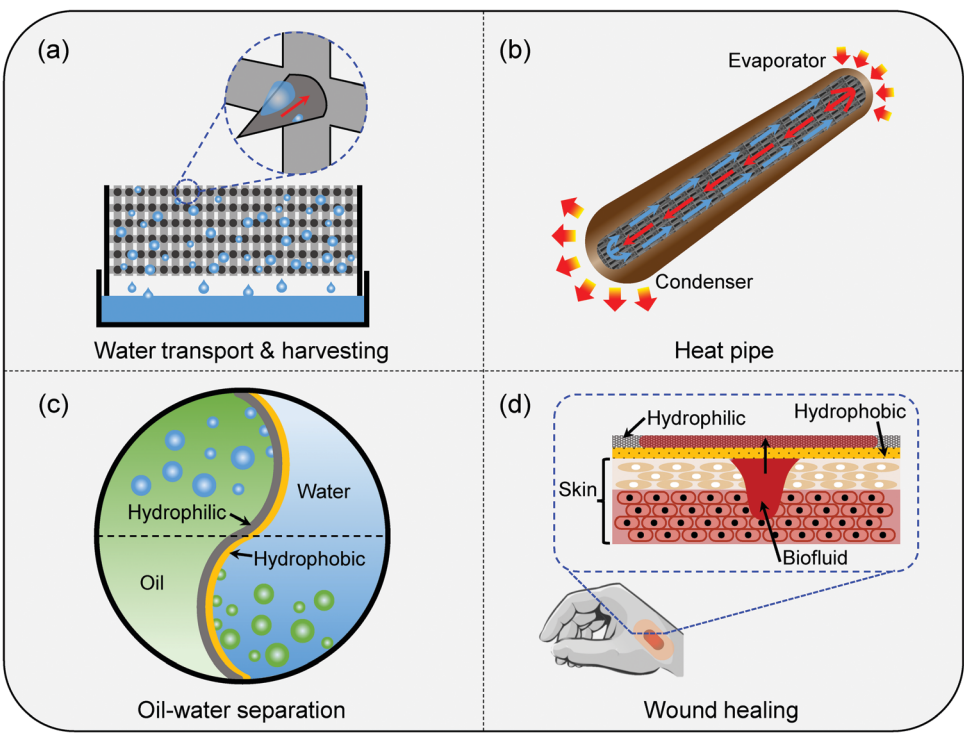

Fig. 9 Representative applications of engineered liquid diodes. (a) Schematic diagram of water transport and harvesting using woven nets featuring conical structure arrays. (b) Schematic diagram of a heat pipe using a topological liquid diode. (c) Schematic image showing the application of oil–water separation using a Janus membrane. (d) Schematic image showing the application of wound healing by virtue of a Janus membrane.

6. Conclusions and perspectives

Developing effective strategies to achieve preferential liquid transport has been scientifically and practically important. Due to the limitation in the length, our review mainly focuses on elaborating how to engineer liquid diodes using a biomimetic approach. It is expected that with the convergence of biomimetics, materials science, and manufacturing, a diversity of liquid diodes with preferred functions will be developed and significantly shape the way for liquid transport.

Further progress in mimicking biological surfaces to advance the development of engineered liquid diodes demands a deep fundamental understanding of transport dynamics in a confined space at a small scale. Despite advances in various visualization techniques, it is difficult to observe and explore the nanoscale transport dynamics on biological surfaces and thus much important information at the bottom remains to be uncovered. On the other hand, the transport dynamics on biological surfaces are subjected to dynamic environmental conditions. The directional liquid transport on natural surfaces might collapse under harsh environmental conditions, such as heavy rain, strong wind and high humidity. More importantly, biological materials have evolved superior functions to combat challenging conditions including self-healing, self-cleaning, antifouling and stimulus-based responses. In the future, more efforts shall be devoted to exploiting such particular abilities that efficiently increase the robustness of directional transport on biological surfaces. Moreover, in nature, protein channels take advantage of delicate separation mechanisms, including size exclusion and electrostatic repulsion, for selective water and ion transport. It will be more exciting to create artificial structures that replicate the feat achieved by nature in protein channels.[158]

Many fundamental challenges need to be addressed before adaptation to various practical applications. For example, how to overcome the hysteresis resistance that strikingly retards the self-transport of a liquid on engineered liquid diodes. The transport distance and speed on engineered liquid diodes are significantly limited owing to the presence of hysteresis resistance. Thus in many applications, external thermal, electrical, optical, magnetic or mechanical energy is usually applied to transport liquids on responsive materials.[159–168] But, such active strategies are subject to limitations from the consumption of external energy and selection of stimuli-responsive materials, which in turn restrict their wide applications. On the other hand, SLIPs might serve as a promising and efficient platform for the transport of various droplets almost without suffering from the hysteresis force with respect to solid substrates.[73–75,77,80,169–174] In particular, hydrophilic SLIPs are capable of rapidly nucleating and directionally removing water droplets by coupling with nanotextured directional microgrooves. Recent studies also reveal that engineered liquid diodes pre-wetted by a thin layer of water film enable superfast transport of liquids with respect to dry liquid diodes.[24,39,175]

Advanced manufacturing techniques are also important for the development of novel fluidic devices. Recently, the 3D printing technique[176–178] has gained increasing attention owing to its advantage of translating computer-aided programmable design into desired 3D structures in an on-demand manner. However, its limited resolution also restricts the development of refined structures to achieve advanced functions such as selective rectification and rejection of liquids and ions. Moreover, 3D printing is limited to a few responsive materials such as thermoplastics, thermosets, elastomers and functional polymers. Thus it is impossible to develop a general manufacturing technique which is versatile enough to satisfy all needs.[179] Moreover, the choice and optimization of scalable, cost-effective manufacturing techniques to engineer liquid diodes should be based on a diversity of factors.

Conflicts of interest

There are no conflicts of interest to declare.

Acknowledgements

Z. W. is grateful for financial support from the Research Grants Council of Hong Kong (No. C1018-17G, 11275216 and 11218417) and City University of Hong Kong (No. 9360140 and 9667139).

References

1 A. A. Darhuber and S. M. Troian, *Annu. Rev. Fluid Mech.*, 2005, **37**, 425–455.
2 M. K. Chaudhury, A. Chakrabarti and S. Daniel, *Langmuir*, 2015, **31**, 9266–9281.
3 X. Xu and T. Qian, *Phys. Rev. E: Stat., Nonlinear, Soft Matter Phys.*, 2012, **85**, 051601.
4 Y. Zhao, H. Wang, H. Zhou and T. Lin, *Small*, 2017, **13**, 1601070.
5 J. Li and Z. Guo, *Nanoscale*, 2018, **10**, 13814–13831.
6 J. Li, Y. Hou, Y. Liu, C. Hao, M. Li, M. K. Chaudhury, S. Yao and Z. Wang, *Nat. Phys.*, 2016, **12**, 606–612.
7 H.-C. Yang, J. Hou, V. Chen and Z.-K. Xu, *Angew. Chem., Int. Ed.*, 2016, **55**, 13398–13407.
8 S. Zhang, J. Huang, Z. Chen, S. Yang and Y. Lai, *J. Mater. Chem. A*, 2019, **7**, 38–63.
9 N. J. Cira, A. Benusiglio and M. Prakash, *Nature*, 2015, **519**, 446–450.
10 W. S. Wong, M. Li, D. R. Nisbet, V. S. Craig, Z. Wang and A. Tricoli, *Sci. Adv.*, 2016, **2**, e1600417.
11 T. M. Schutzius, S. Jung, T. Maitra, G. Graeber, M. Köhme and D. Poulikakos, *Nature*, 2015, **527**, 82–85.
12 A. Bouillant, T. Mouterde, P. Bourrianne, A. Lagarde, C. Clanet and D. Quéré, *Nat. Phys.*, 2018, **14**, 1188–1192.
13 J. Y. Huang, Y.-C. Lo, J. J. Niu, A. Kushima, X. Qian, L. Zhong, S. X. Mao and J. Li, *Nat. Nanotechnol.*, 2013, **8**, 277–281.
14 J. Li, J. Li, J. Sun, S. Feng and Z. Wang, *Adv. Mater.*, 2019, **0**, 1806501.
15 M. K. Chaudhury and G. M. Whitesides, *Science*, 1992, **256**, 1539–1541.

16 A. R. Parker and C. R. Lawrence, *Nature*, 2001, **414**, 33–34.
17 F. T. Malik, R. M. Clement, D. T. Gethin, D. Beysens, R. E. Cohen, W. Krawszik and A. R. Parker, *Bioinspiration Biomimetics*, 2015, **10**, 036005.
18 Y. Zheng, H. Bai, Z. Huang, X. Tian, F.-Q. Nie, Y. Zhao, J. Zhai and L. Jiang, *Nature*, 2010, **463**, 640–643.
19 J. Ju, H. Bai, Y. Zheng, T. Zhao, R. Fang and L. Jiang, *Nat. Commun.*, 2012, **3**, 1247.
20 M. Prakash, D. Quéré and J. W. Bush, *Science*, 2008, **320**, 931–934.
21 P. Comanns, G. Buchberger, A. Buchsbaum, R. Baumgartner, A. Kogler, S. Bauer and W. Baumgartner, *J. R. Soc., Interface*, 2015, **12**, 20150415.
22 H. Chen, P. Zhang, L. Zhang, H. Liu, Y. Jiang, D. Zhang, Z. Han and L. Jiang, *Nature*, 2016, **532**, 85–89.
23 Z. Pan, W. G. Pitt, Y. Zhang, N. Wu, Y. Tao and T. T. Truscott, *Nat. Plants*, 2016, **2**, 16076.
24 D. Chen, S. Niu, J. Zhang, Z. Mu, H. Chen, D. Zhang, Z. Yao, Z. Han and L. Ren, *Adv. Mater. Interfaces*, 2018, **5**, 1800802.
25 K.-H. Chu, R. Xiao and E. N. Wang, *Nat. Mater.*, 2010, **9**, 413–417.
26 J. Li, X. Zhou, J. Li, L. Che, J. Yao, G. McHale, M. K. Chaudhury and Z. Wang, *Sci. Adv.*, 2017, **3**, eaao3530.
27 V. Jokinen, M. Leinikka and S. Franssila, *Adv. Mater.*, 2009, **21**, 4835–4838.
28 Y. Lin, Z. Hu, C. Gao, Z. Guo, C. Li and Y. Zheng, *Adv. Mater. Interfaces*, 2018, **5**, 1800962.
29 Y. Si, T. Wang, C. Li, C. Yu, N. Li, C. Gao, Z. Dong and L. Jiang, *ACS Nano*, 2018, **12**, 9214–9222.
30 X. M. Yang, Z. W. Zhong, E. Q. Li, Z. H. Wang, W. Xu, S. T. Thoroddsen and X. X. Zhang, *Soft Matter*, 2013, **9**, 11113–11119.
31 C. Li, N. Li, X. Zhang, Z. Dong, H. Chen and L. Jiang, *Angew. Chem., Int. Ed.*, 2016, **55**, 14988–14992.
32 L. Shang, Y. Yu, W. Gao, Y. Wang, L. Qu, Z. Zhao, R. Chai and Y. Zhao, *Adv. Funct. Mater.*, 2018, **28**, 1705802.
33 M. Reyssat, F. Pardo and D. Quéré, *Europhys. Lett.*, 2009, **87**, 36003.
34 C. Liu, J. Sun, J. Li, C. Xiang, L. Che, Z. Wang and X. Zhou, *Sci. Rep.*, 2017, **7**, 7552.
35 E. Lorenceau and D. Quéré, *J. Fluid Mech.*, 2004, **510**, 29–45.
36 P. Renvoisé, J. W. M. Bush, M. Prakash and D. Quéré, *Europhys. Lett.*, 2009, **86**, 64003.
37 X. Heng and C. Luo, *Langmuir*, 2015, **31**, 2743–2748.
38 C. Lv, C. Chen, Y.-C. Chuang, F.-G. Tseng, Y. Yin, F. Grey and Q. Zheng, *Phys. Rev. Lett.*, 2014, **113**, 026101.
39 E. Q. Li and S. T. Thoroddsen, *Phys. Fluids*, 2013, **25**, 052105.
40 S. Li, J. Liu and J. Hou, *Sci. Rep.*, 2016, **6**, 37888.
41 R. W. Style, Y. Che, S. J. Park, B. M. Weon, J. H. Je, C. Hyland, G. K. German, M. P. Power, L. A. Wilen, J. S. Wettlaufer and E. R. Dufresne, *Proc. Natl. Acad. Sci. U. S. A.*, 2013, **110**, 12541–12544.
42 H. Wang, J. Ding, L. Dai, X. Wang and T. Lin, *J. Mater. Chem.*, 2010, **20**, 7938–7940.
43 X. Tian, H. Jin, J. Sainio, R. H. A. Ras and O. Ikkala, *Adv. Funct. Mater.*, 2014, **24**, 6023–6028.
44 J. E. Mates, T. M. Schutzius, J. Qin, D. E. Waldroup and C. M. Megaridis, *ACS Appl. Mater. Interfaces*, 2014, **6**, 12837–12843.
45 J. Wu, N. Wang, L. Wang, H. Dong, Y. Zhao and L. Jiang, *Soft Matter*, 2012, **8**, 5996–5999.
46 K. Liu, Z. Huang, A. Hemmatifar, D. I. Oyarzun, J. Zhou and J. G. Santiago, *ACS Appl. Mater. Interfaces*, 2018, **10**, 26759–26764.
47 F. Ren, G. Li, Z. Zhang, X. Zhang, H. Fan, C. Zhou, Y. Wang, Y. Zhang, C. Wang, K. Mu, Y. Su and D. Wu, *J. Mater. Chem. A*, 2017, **5**, 18403–18408.
48 T. Young, *Philos. Trans. R. Soc. London*, 1805, **95**, 65–87.
49 J. W. Gibbs, *Am. J. Sci.*, 1878, **3**, 441–458.
50 H. Eral and J. Oh, *Colloid Polym. Sci.*, 2013, **291**, 247–260.
51 M. Nosonovsky, *J. Chem. Phys.*, 2007, **126**, 224701.
52 R. Tadmor, *Langmuir*, 2004, **20**, 7659–7664.
53 R. N. Wenzel, *Ind. Eng. Chem.*, 1936, **28**, 988–994.
54 A. B. D. Cassie, *Discuss. Faraday Soc.*, 1948, **3**, 11–16.
55 A. B. D. Cassie and S. Baxter, *Trans. Faraday Soc.*, 1944, **40**, 546–551.
56 W. Barthlott and C. Neinhuis, *Planta*, 1997, **202**, 1–8.
57 C. Neinhuis and W. Barthlott, *Ann. Bot.*, 1997, **79**, 667–677.
58 T. S. John, R. H. Scott and A. Tolga, *Rep. Prog. Phys.*, 2015, **78**, 086501.
59 K. Liu and L. Jiang, *Nanoscale*, 2011, **3**, 825–838.
60 Y. Si and Z. Guo, *Nanoscale*, 2015, **7**, 5922–5946.
61 R. Hensel, R. Helbig, S. Aland, H. G. Braun, A. Voigt, C. Neinhuis and C. Werner, *Langmuir*, 2013, **29**, 1100–1112.
62 T. Liu and C.-J. Kim, *Science*, 2014, **346**, 1096–1100.
63 A. Tuteja, W. Choi, M. Ma, J. M. Mabry, S. A. Mazzella, G. C. Rutledge, G. H. McKinley and R. E. Cohen, *Science*, 2007, **318**, 1618–1622.
64 A. Tuteja, W. Choi, J. M. Mabry, G. H. McKinley and R. E. Cohen, *Proc. Natl. Acad. Sci. U. S. A.*, 2008, **105**, 18200–18205.
65 R. Hensel, C. Neinhuis and C. Werner, *Chem. Soc. Rev.*, 2016, **45**, 323–341.
66 P. Zhu, T. Kong, X. Tang and L. Wang, *Nat. Commun.*, 2017, **8**, 15823.
67 Z. Wang, C. Lopez, A. Hirsa and N. Koratkar, *Appl. Phys. Lett.*, 2007, **91**, 023105.
68 Y. Liu, L. Moevius, X. Xu, T. Qian, J. M. Yeomans and Z. Wang, *Nat. Phys.*, 2014, **10**, 515–519.
69 D. Richard, C. Clanet and D. Quéré, *Nature*, 2002, **417**, 811.
70 J. C. Bird, R. Dhiman, H.-M. Kwon and K. K. Varanasi, *Nature*, 2013, **503**, 385–388.
71 Y. Liu, M. Andrew, J. Li, J. M. Yeomans and Z. Wang, *Nat. Commun.*, 2015, **6**, 10034.
72 A. Gauthier, S. Symon, C. Clanet and D. Quéré, *Nat. Commun.*, 2015, **6**, 8001.
73 T. S. Wong, S. H. Kang, S. K. Y. Tang, E. J. Smythe, B. D. Hatton, A. Grinthal and J. Aizenberg, *Nature*, 2011, **477**, 443–447.
74 A. Lafuma and D. Quéré, *Europhys. Lett.*, 2011, **96**, 56001.

75 S. Anand, A. T. Paxson, R. Dhiman, J. D. Smith and K. K. Varanasi, *ACS Nano*, 2012, **6**, 10122–10129.
76 P. Kim, T. S. Wong, J. Alvarenga, M. J. Kreder, W. E. Adorno-Martinez and J. Aizenberg, *ACS Nano*, 2012, **6**, 6569–6577.
77 P. Irajizad, M. Hasnain, N. Farokhnia, S. M. Sajadi and H. Ghasemi, *Nat. Commun.*, 2016, **7**, 13395.
78 J. Wang, L. Sun, M. Zou, W. Gao, C. Liu, L. Shang, Z. Gu and Y. Zhao, *Sci. Adv.*, 2017, **3**, e1700004.
79 C. Hao, Y. Liu, X. Chen, Y. He, Q. Li, K. Y. Li and Z. Wang, *Sci. Rep.*, 2014, **4**, 6846.
80 X. Dai, N. Sun, S. O. Nielsen, B. B. Stogin, J. Wang, S. Yang and T.-S. Wong, *Sci. Adv.*, 2018, **4**, eaaq0919.
81 C. Hao, J. Li, Y. Liu, X. Zhou, Y. Liu, R. Liu, L. Che, W. Zhou, D. Sun, L. Li, L. Xu and Z. Wang, *Nat. Commun.*, 2015, **6**, 7986.
82 B. Bhushan, *Philos. Trans. R. Soc., A*, 2009, **367**, 1445–1486.
83 K. Koch, B. Bhushan and W. Barthlott, *Prog. Mater. Sci.*, 2009, **54**, 137–178.
84 P. Comanns, C. Effertz, F. Hischen, K. Staudt, W. Böhme and W. Baumgartner, *Beilstein J. Nanotechnol.*, 2011, **2**, 204–214.
85 H. F. Bohn and W. Federle, *Proc. Natl. Acad. Sci. U. S. A.*, 2004, **101**, 14138–14143.
86 J. Li, H. Zheng, Z. Yang and Z. Wang, *Commun. Phys.*, 2018, **1**, 35.
87 O. Bliznyuk, H. P. Jansen, E. S. Kooij, H. J. W. Zandvliet and B. Poelsema, *Langmuir*, 2011, **27**, 11238–11245.
88 O. Bliznyuk, J. R. T. Seddon, V. Veligura, E. S. Kooij, H. J. W. Zandvliet and B. Poelsema, *ACS Appl. Mater. Interfaces*, 2012, **4**, 4141–4148.
89 D. Hong, W. K. Cho, B. Kong and I. S. Choi, *Langmuir*, 2010, **26**, 15080–15083.
90 Y. Ito, M. Heydari, A. Hashimoto, T. Konno, A. Hirasawa, S. Hori, K. Kurita and A. Nakajima, *Langmuir*, 2007, **23**, 1845–1850.
91 N. Moumen, R. S. Subramanian and J. B. McLaughlin, *Langmuir*, 2006, **22**, 2682–2690.
92 J. Zhang and Y. Han, *Langmuir*, 2007, **23**, 6136–6141.
93 X. Zhu, H. Wang, Q. Liao, Y. D. Ding and Y. B. Gu, *Exp. Therm. Fluid Sci.*, 2009, **33**, 947–954.
94 S. Daniel, M. K. Chaudhury and J. C. Chen, *Science*, 2001, **291**, 633–636.
95 S. Morgenthaler, C. Zink and N. D. Spencer, *Soft Matter*, 2008, **4**, 419–434.
96 J. Genzer, *Annu. Rev. Mater. Res.*, 2012, **42**, 435–468.
97 H. S. Khoo and F.-G. Tseng, *Appl. Phys. Lett.*, 2009, **95**, 063108.
98 J. Li, X. L. Tian, A. P. Perros, S. Franssila and V. Jokinen, *Adv. Mater. Interfaces*, 2014, **1**, 1400001.
99 N. Moradi, F. Varnik and I. Steinbach, *Europhys. Lett.*, 2010, **89**, 26006.
100 A. Shastry, M. J. Case and K. F. Böhringer, *Langmuir*, 2006, **22**, 6161–6167.
101 C. Sun, X.-W. Zhao, Y.-H. Han and Z.-Z. Gu, *Thin Solid Films*, 2008, **516**, 4059–4063.
102 J. Wu, R. Ma, Z. Wang and S. Yao, *Appl. Phys. Lett.*, 2011, **98**, 204104.
103 J.-T. Yang, Z.-H. Yang, C.-Y. Chen and D.-J. Yao, *Langmuir*, 2008, **24**, 9889–9897.
104 C. Liu, J. Sun, Y. Zhuang, J. Wei, J. Li, L. Dong, D. Yan, A. Hu, X. Zhou and Z. Wang, *Nanoscale*, 2018, **10**, 23164–23169.
105 S. Daniel, M. K. Chaudhury and P. G. de Gennes, *Langmuir*, 2005, **21**, 4240–4248.
106 S. Daniel and M. K. Chaudhury, *Langmuir*, 2002, **18**, 3404–3407.
107 M. K. Chaudhury and P. S. Goohpattader, *Eur. Phys. J. E: Soft Matter Biol. Phys.*, 2013, **36**, 15.
108 J. Li, Q. H. Qin, A. Shah, R. H. Ras, X. Tian and V. Jokinen, *Sci. Adv.*, 2016, **2**, e1600148.
109 J. Bueno, Y. Bazilevs, R. Juanes and H. Gomez, *Extreme Mech. Lett.*, 2017, **13**, 10–16.
110 S. Karpitschka, A. Pandey, L. A. Lubbers, J. H. Weijs, L. Botto, S. Das, B. Andreotti and J. H. Snoeijer, *Proc. Natl. Acad. Sci. U. S. A.*, 2016, **113**, 7403–7407.
111 X.-P. Zheng, H.-P. Zhao, L.-T. Gao, J.-L. Liu, S.-W. Yu and X.-Q. Feng, *J. Colloid Interface Sci.*, 2008, **323**, 133–140.
112 R. W. Style, A. Jagota, C.-Y. Hui and E. R. Dufresne, *Annu. Rev. Condens. Matter Phys.*, 2016, **8**, 3.1–3.20.
113 E. R. Jerison, Y. Xu, L. A. Wilen and E. R. Dufresne, *Phys. Rev. Lett.*, 2011, **106**, 186103.
114 S. Karpitschka, S. Das, M. van Gorcum, H. Perrin, B. Andreotti and J. H. Snoeijer, *Nat. Commun.*, 2015, **6**, 7891.
115 L. Guo and G. H. Tang, *Int. J. Heat Mass Transfer*, 2015, **84**, 198–202.
116 R. Hanumanthu and K. J. Stebe, *Colloids Surf., A*, 2006, **282**, 227–239.
117 Y.-E. Liang, H.-K. Tsao and Y.-J. Sheng, *Langmuir*, 2015, **31**, 1704–1710.
118 C. Luo, *Langmuir*, 2015, **31**, 11809–11813.
119 M. P. Moody and P. Attard, *Phys. Rev. Lett.*, 2003, **91**, 056104.
120 C. Luo, X. Heng and M. Xiang, *Langmuir*, 2014, **30**, 8373–8380.
121 J. Bico and D. Quéré, *J. Fluid Mech.*, 2002, **467**, 101–127.
122 J.-L. Liu, R. Xia, B.-W. Li and X.-Q. Feng, *Chin. Phys. Lett.*, 2007, **24**, 3210.
123 P. S. Brown and B. Bhushan, *Philos. Trans. R. Soc., A*, 2016, **374**, 20160135.
124 J. Ju, Y. Zheng and L. Jiang, *Acc. Chem. Res.*, 2014, **47**, 2342–2352.
125 S. Zhang, J. Huang, Z. Chen and Y. Lai, *Small*, 2016, **13**, 1602992.
126 H. Zhu, Z. Guo and W. Liu, *Chem. Commun.*, 2016, **52**, 3863–3879.
127 K. Li, J. Ju, Z. Xue, J. Ma, L. Feng, S. Gao and L. Jiang, *Nat. Commun.*, 2013, **4**, 2276.
128 B. Ai, L. Wang, H. Mohwald, Y. Yu, Z. Zhao, Z. Zhou, G. Zhang and Q. Lin, *Sci. Rep.*, 2014, **4**, 6751.
129 T.-i. Kim and K. Y. Suh, *Soft Matter*, 2009, **5**, 4131–4135.
130 M. K. Kwak, H.-E. Jeong, T.-i. Kim, H. Yoon and K. Y. Suh, *Soft Matter*, 2010, **6**, 1849–1857.
131 C. Plamadeala, F. Hischen, R. Friesenecker, R. Wollhofen, J. Jacak, G. Buchberger, E. Heiss, T. A. Klar, W. Baumgartner and J. Heitz, *R. Soc. Open Sci.*, 2017, **4**, 160849.

132 N. A. Malvadkar, M. J. Hancock, K. Sekeroglu, W. J. Dressick and M. C. Demirel, *Nat. Mater.*, 2010, **9**, 1023–1028.
133 Y. Lin, Z. Hu, M. Zhang, T. Xu, S. Feng, L. Jiang and Y. Zheng, *Adv. Funct. Mater.*, 2018, **28**, 1800163.
134 M. J. Hancock, K. Sekeroglu and M. C. Demirel, *Adv. Funct. Mater.*, 2012, **22**, 2223–2234.
135 M. Zhang, L. Wang, Y. Hou, W. Shi, S. Feng and Y. Zheng, *Adv. Mater.*, 2015, **27**, 5057–5062.
136 H. Chen, L. Zhang, P. Zhang, D. Zhang, Z. Han and L. Jiang, *Small*, 2017, **13**, 1601676.
137 H. W. Chen, L. W. Zhang, Y. Zhang, P. F. Zhang, D. Y. Zhang and L. Jiang, *J. Mater. Chem. A*, 2017, **5**, 6914–6920.
138 P. Zhang, H. Chen, L. Li, H. Liu, G. Liu, L. Zhang, D. Zhang and L. Jiang, *ACS Appl. Mater. Interfaces*, 2017, **9**, 5645–5652.
139 P. Zhang, L. Zhang, H. Chen, Z. Dong and D. Zhang, *Adv. Mater.*, 2017, **29**, 1702995.
140 G. Buchberger, F. Hischen, P. Comanns, R. Baumgartner, A. Kogler, A. Buchsbaum, S. Bauer and W. Baumgartner, *Procedia Eng.*, 2015, **120**, 106–111.
141 G. Buchberger, R. Baumgartner, A. Kogler, T. Fritz, S. Bauer and W. Baumgartner, *Sens. Actuators, A*, 2018, **283**, 375–385.
142 C. Li, C. Yu, D. Hao, L. Wu, Z. Dong and L. Jiang, *Adv. Funct. Mater.*, 2018, **28**, 1707490.
143 J. Berthier, F. Loe-Mie, V. M. Tran, S. Schoumacker, F. Mittler, G. Marchand and N. Sarrut, *J. Colloid Interface Sci.*, 2009, **338**, 296–303.
144 J. F. Oliver, C. Huh and S. G. Mason, *J. Colloid Interface Sci.*, 1977, **59**, 568–581.
145 H.-C. Yang, Y. Xie, J. Hou, A. K. Cheetham, V. Chen and S. B. Darling, *Adv. Mater.*, 2018, **30**, 1801495.
146 S. Feng, Y. Xing, S. Deng, W. Shang, D. Li, M. Zhang, Y. Hou and Y. Zheng, *Adv. Mater. Interfaces*, 2018, **5**, 1701193.
147 P. Gupta and B. Kandasubramanian, *ACS Appl. Mater. Interfaces*, 2017, **9**, 19102–19113.
148 Z. Wang, Y. Wang and G. Liu, *Angew. Chem., Int. Ed.*, 2016, **55**, 1291–1294.
149 H. Zhou, H. Wang, H. Niu and T. Lin, *Sci. Rep.*, 2013, **3**, 2964.
150 M. Cao, J. Xiao, C. Yu, K. Li and L. Jiang, *Small*, 2015, **11**, 4379–4384.
151 H. Wang, H. Zhou, H. Niu, J. Zhang, Y. Du and T. Lin, *Adv. Mater. Interface*s, 2015, **2**, 1400506.
152 R. Hu, N. Wang, L. Hou, Z. Cui, J. Liu, D. Li, Q. Li, H. Zhang and Y. Zhao, *J. Mater. Chem. A*, 2019, **7**, 124–132.
153 K.-C. Park, S. S. Chhatre, S. Srinivasan, R. E. Cohen and G. H. McKinley, *Langmuir*, 2013, **29**, 13269–13277.
154 T. Xu, Y. Lin, M. Zhang, W. Shi and Y. Zheng, *ACS Nano*, 2016, **10**, 10681–10688.
155 R. Savino and D. Paterna, *Phys. Fluids*, 2006, **18**, 118103.
156 Y. Cheng and Z. Wang, *Natl. Sci. Rev.*, 2019, **0**, 1–2.
157 L. Shi, X. Liu, W. Wang, L. Jiang and S. Wang, *Adv. Mater.*, 2018, **0**, 1804187.
158 K. Gopinadhan, S. Hu, A. Esfandiar, M. Lozada-Hidalgo, F. C. Wang, Q. Yang, A. V. Tyurnina, A. Keerthi, B. Radha and A. K. Geim, *Science*, 2019, **363**, 145–148.
159 M. Frieder and B. Jean-Christophe, *J. Phys.: Condens. Matter*, 2005, **17**, R705.
160 W. C. Nelson and C.-J. C. Kim, *J. Adhes. Sci. Technol.*, 2012, **26**, 1747–1771.
161 N. A. Malvadkar, M. J. Hancock, K. Sekeroglu, W. J. Dressick and M. C. Demirel, *Nat. Mater.*, 2010, **9**, 1023–1028.
162 X. Noblin, R. Kofman and F. Celestini, *Phys. Rev. Lett.*, 2009, **102**, 194504.
163 K. Ichimura, S. K. Oh and M. Nakagawa, *Science*, 2000, **288**, 1624–1626.
164 G. Kwon, D. Panchanathan, S. R. Mahmoudi, M. A. Gondal, G. H. McKinley and K. K. Varanasi, *Nat. Commun.*, 2017, **8**, 14968.
165 J. A. Lv, Y. Liu, J. Wei, E. Chen, L. Qin and Y. Yu, *Nature*, 2016, **537**, 179–184.
166 A. Egatz-Gómez, S. Melle, A. A. García, S. A. Lindsay, M. Márquez, P. Domínguez-García, M. A. Rubio, S. T. Picraux, J. L. Taraci, T. Clement, D. Yang, M. A. Hayes and D. Gust, *Appl. Phys. Lett.*, 2006, **89**, 034106.
167 L. Y. Yeo and J. R. Friend, *Biomicrofluidics*, 2009, **3**, 012002.
168 J. B. Brzoska, F. Brochard-Wyart and F. Rondelez, *Langmuir*, 1993, **9**, 2220–2224.
169 D. Daniel, J. V. I. Timonen, R. P. Li, S. J. Velling and J. Aizenberg, *Nat. Phys.*, 2017, **13**, 1020–1025.
170 X. Dai, B. B. Stogin, S. Yang and T.-S. Wong, *ACS Nano*, 2015, **9**, 9260–9267.
171 J. Hui Guan, E. Ruiz-Gutierrez, B. B. Xu, D. Wood, G. McHale, R. Ledesma-Aguilar and G. George Wells, *Soft Matter*, 2017, **13**, 3404–3410.
172 N. Bjelobrk, H.-L. Girard, S. B. Subramanyam, H.-M. Kwon, D. Quéré and K. K. Varanasi, *Phys. Rev. Fluids*, 2016, **1**, 063902.
173 J. D. Smith, R. Dhiman, S. Anand, E. Reza-Garduno, R. E. Cohen, G. H. McKinley and K. K. Varanasi, *Soft Matter*, 2013, **9**, 1772–1780.
174 K. C. Park, P. Kim, A. Grinthal, N. He, D. Fox, J. C. Weaver and J. Aizenberg, *Nature*, 2016, **531**, 78–82.
175 H. Chen, T. Ran, Y. Gan, J. Zhou, Y. Zhang, L. Zhang, D. Zhang and L. Jiang, *Nat. Mater.*, 2018, **17**, 935–942.
176 R. L. Truby and J. A. Lewis, *Nature*, 2016, **540**, 371–378.
177 Y. Zhang, F. Zhang, Z. Yan, Q. Ma, X. Li, Y. Huang and J. A. Rogers, *Nat. Rev. Mater.*, 2017, **2**, 17019.
178 S. C. Ligon, R. Liska, J. Stampfl, M. Gurr and R. Mülhaupt, *Chem. Rev.*, 2017, **117**, 10212–10290.
179 U. G. K. Wegst, H. Bai, E. Saiz, A. P. Tomsia and R. O. Ritchie, *Nat. Mater.*, 2015, **14**, 23–36.